


Redesigned Spatial Modulation for Spatially Correlated Fading Channels

G. D. Goutham Simha¹  · Shriharsha Koila¹ · N. Neha¹ ·
M. A. N. S. Raghavendra¹ · U. Sripathi¹

Published online: 11 August 2017
© Springer Science+Business Media, LLC 2017

Abstract In this paper, a new variant of Spatial Modulation (SM) Multiple-Input Multiple-Output (MIMO) transmission technique, designated as Redesigned Spatial Modulation (ReSM) has been proposed. In ReSM scheme, a dynamic mapping for antenna selection is adopted. This scheme employs both single antenna as well as double antenna combinations depending upon channel conditions to combat the effect of spatial correlation. When evaluated over spatially correlated channel conditions, for a fixed spectral efficiency and number of transmit antennas, ReSM exhibits performance improvement of at least 3 dB over all the conventional SM schemes including Trellis Coded Spatial Modulation (TCSM) scheme. Furthermore, a closed form expression for the upper bound on Pairwise Error Probability (PEP) for ReSM has been derived. This has been used to calculate the upper bound for the Average Bit Error Probability (ABEP) for spatially correlated channels. The results of Monte Carlo simulations are in good agreement with the predictions made by analytical results. The relative gains of all the comparison plots in the paper are specified at an ABER of 10^{-4} .

✉ G. D. Goutham Simha
goutham.mah@gmail.com

Shriharsha Koila
bhatshri29@gmail.com

N. Neha
nehanie2010@gmail.com

M. A. N. S. Raghavendra
mans.raghavendra@rediff.com

U. Sripathi
sripathi.acharya1@gmail.com

¹ Department of Electronics and Communication, National Institute of Technology Karnataka (NITK), Surathkal, Mangalore, India

Keywords Spatially Correlated (SC) · Redesigned SM (ReSM) · Trellis Coded SM (TCSM) · Spatial Multiplexing (SMX) · Spectral Efficiency (η) · Universal Software Radio Peripheral (USRP) · Maximal Receive Ratio Combining (MRRC)

1 Introduction

Wireless communication systems must operate with severe constraints imposed on two major limited resources, power and bandwidth. A number of MIMO techniques were proposed in the early part of the twenty-first century to improve spectral efficiency and/or reliability of communication. However, a drawback of these schemes is that they have not been designed to address the important issue of energy efficiency. In the year 2008, Mesleh et al. [1] proposed a new scheme designated as Spatial Modulation (SM) for MIMO wireless communication systems. SM-MIMO technique was introduced to achieve an exceptional trade-off between spectral efficiency and energy efficiency in MIMO wireless communication systems [1, 2]. Various researchers have analyzed the performance of SM in all possible environments [3]. After quantifying the benefits of SM, researchers have proposed variants of SM which aims to attain improved spectral efficiency without sacrificing energy efficiency. These techniques if deployed, can serve as replacements/alternatives to SMX in battery operated wireless devices.

One of the techniques that has been employed to improve the performance of SM schemes is to activate more than one antennas at any given instant of time. A number of such schemes have been proposed in literature by Abdelhamid Younis et al. [3] such as Generalized SM (GNSM) and Variable Generalized SM (VGSM). A more general approach termed as Improved Spatial Modulation (ISM) or Extended Spatial Modulation (EXSM) was proposed by Luna Rivera et al. in 2012 [4, 5]. In 2014 Chien-Chun Cheng et al. [6, 7] presented another spectrally efficient method called Enhanced Spatial Modulation (ESM) for MIMO systems. In 2014, Mesleh gave an enhanced version of his original technique (SM) which could provide improved spectral efficiency and this was named as Quadrature Spatial Modulation (QSM) [8, 12, 14]. It is generally observed that the performance of all SM schemes deteriorate under Spatially Correlated (SC) fading channel conditions. To combat the effect of SC, Trellis Coded Spatial Modulation (TCSM) was introduced by Mesleh et al. in [9]. In TCSM the effect of correlation on the performance of SM can be minimized by segregating antennas into subsets, which provide a maximum spatial separation between the antennas in the same subset, although a minimum of four transmit antennas are required to form the subsets. For a system with spectral efficiency of 4 bits per channel use (bpcu), it has been shown that TCSM 4×4 , with hard decision Viterbi decoding and 8QAM provides an improvement of ~ 2 dB over uncoded SM 4×4 system employing QPSK modulation in channels with appreciable correlation. Increasing the spectral efficiency in TCSM, requires an increase in the rate of the convolution code or the order of the modulation scheme. In compact handheld gadgets, placing more than 4 transmit antennas working in a same frequency band is a challenging task principally due to space requirements. An increase in spectral efficiency brought about by the use of higher order modulation schemes with the number of transmit antennas kept constant, will result in a deterioration in the BER performance. Improved SM (ISM) [4, 5] is another SM technique that is designed to employ variable number of transmit antennas. It provides an increase in spectral efficiency and performance gain of ~ 2 dB as compared to conventional SM when employed over uncorrelated channel environments. However, in

the presence of channel correlation, a performance deterioration of ~ 2 dB over SM is also observed. Inspired by the principles of TCSM and ISM, we have proposed a new scheme, named Redesigned Spatial Modulation (ReSM), for spatially correlated fading environments. This scheme has been designed to employ the concept of simultaneous transmission of different symbols via multiple collocated antennas. It also maximizes the Euclidean distance between active spatial bits which in turn serve to reduce the ambiguities in their recovery at the receiver end. The number of transmit antennas in ReSM must be a power of 2. The major advantage of ReSM compared with TCSM is that ReSM does not require any additional channel encoder/decoder (error correcting code). ReSM schemes combine well with the high end utilities and services provided by 4G systems. In SC fading environment, coded scheme (TCSM) perform better by about 3 dB as compared with uncoded SM schemes [11]. In this work we have designed ReSM to ensure reliable transmission for spectral efficiency of 6 bpcu. We show that uncoded ReSM scheme can significantly outperform TCSM over SC channels (SNR gain over TCSM is ~ 3 dB). The specific contributions of this paper are:

- Design and performance evaluation of ReSM, determination of suitability of ReSM in SC channel environments.
- Real time indoor measurements leading to determination of channel coefficients under close antenna spacing.
- Derivation of a closed form expression for the PEP and extension of this result to obtain an upper bound on the ABEP.

The rest of the paper is organized as follows: Section 2 presents a brief introduction to the channel models which are used to describe channels exhibiting spatial correlation. Later system models are described in Sect. 3. A construction of ReSM scheme is described in Sect. 4 followed by an analytical treatment of ReSM in Sect. 5. Section 6 presents a comparison of receiver computational complexity across various SM schemes. Section 7 presents the simulation results and real time indoor measurements employing USRP B210. Finally the paper is concluded in Sect. 8.

2 Channel Models

A number of mathematical models have been proposed in literature to describe the behavior of channel perturbations introduced by the wireless channel operating over different frequencies in different physical environments. Our primary interest is on spatially correlated channels with and without LOS components. We have used Kronecker model [3, 9, 21] to describe spatial correlation. A brief description follows.

2.1 Spatial Correlation Channel Model

In wireless communication, the occurrence of spatial correlation depends on channel environment and spacing between the antenna elements [17]. In compact handheld wireless devices required spacing between the antenna elements within a single antenna array (either transmit or receive) cannot be guaranteed. Apparently it becomes necessary to consider spatial correlations among the channels, which describe the behavior of antenna elements within an array. Using clustered channel model, the correlation between signals

from any two antenna elements \mathbf{m}, \mathbf{n} within an array is determined as $\mathbf{R}_{(\mathbf{m},\mathbf{n})}$ given in [17, 21].

$$\mathbf{R}_{(\mathbf{m},\mathbf{n})} = \frac{e^{j(D(\mathbf{m}-\mathbf{n}) \sin(\theta_0))}}{1 + \frac{\sigma_\theta^2}{2} [(D(\mathbf{m} - \mathbf{n}) \cos(\theta_0))]^2}; \quad \mathbf{m}, \mathbf{n} \in \{1, 2, 3, \dots, N_t\} \tag{1}$$

here $D = \frac{2\pi d_a}{\lambda}$ where d_a is the distance of separation between the antenna elements, λ is the wavelength of operation, θ_0 and σ_θ are the Angle of Arrival (AOA) and Angular Spread (AS) respectively. Using (1), the transmit correlation and receive correlation matrices can be expressed as \mathbf{R}_{TRAN} , \mathbf{R}_{REC} and are computed as shown in (2) and (3). The transmit correlation matrix \mathbf{R}_{TRAN} contains information about the correlation between different antenna elements of the transmit array and the receive correlation matrix \mathbf{R}_{REC} specifies the correlation between various elements of the receive antenna array.

$$\mathbf{R}_{\text{TRAN}} = \begin{bmatrix} \mathbf{R}_{(1,1)} & \mathbf{R}_{(1,2)} & \dots & \mathbf{R}_{(1,N_t)} \\ \mathbf{R}_{(2,1)} & \cdot & \cdot & \cdot \\ \vdots & \cdot & \cdot & \cdot \\ \mathbf{R}_{(N_t,1)} & \mathbf{R}_{(N_t,2)} & \dots & \mathbf{R}_{(N_t,N_t)} \end{bmatrix} \tag{2}$$

$$\mathbf{R}_{\text{REC}} = \begin{bmatrix} \mathbf{R}_{(1,1)} & \mathbf{R}_{(1,2)} & \dots & \mathbf{R}_{(1,N_r)} \\ \mathbf{R}_{(2,1)} & \cdot & \cdot & \cdot \\ \vdots & \cdot & \cdot & \cdot \\ \mathbf{R}_{(N_r,1)} & \mathbf{R}_{(N_r,2)} & \dots & \mathbf{R}_{(N_r,N_r)} \end{bmatrix} \tag{3}$$

In order to compute \mathbf{R}_{REC} , the mean AOA is replaced by the mean angle of departure (AOD). Throughout our simulations we have considered the values of mean AOA, AS and mean AOD as indicated in [17, 21]. The realization of SC channel conditions are based on the Kronecker model as shown in [3, 9, 21]. The entries of the channel matrix \mathbf{H} are modeled as complex independent and identically distributed (i.i.d) Gaussian random variables with zero mean and unit variance.

$$\mathbf{H}_c = \mathbf{R}_{\text{REC}}^{1/2} \mathbf{H} \mathbf{R}_{\text{TRAN}}^{1/2} \tag{4}$$

where \mathbf{H}_c is a correlated channel matrix. \mathbf{H} denotes a Rayleigh channel matrix having dimensions $N_r \times N_t$.

2.2 Rician Fading Channel

The Rician distribution is used to model the fading signal amplitude in presence of a considerable LOS component. The entries of channel matrix \mathbf{H} are modeled as given in [3].

$$\mathbf{H}_c = \sqrt{\frac{K}{1+K}} \bar{\mathbf{H}} + \sqrt{\frac{1}{1+K}} \mathbf{H} \tag{5}$$

In the above expression, K is termed as Rician factor, $K/(1+K)$ is the average power of the LOS component $\bar{\mathbf{H}}$ is a matrix of all ones [3, 19, 21], $1/(1+K)$ is the average power of the random component or the scattered component, and \mathbf{H} is a Rayleigh $N_r \times N_t$ matrix whose entries are modeled as complex i.i.d Gaussian random variables with zero mean and unit variance.

3 System Models

3.1 Spatial Modulation (SM)

In SM systems, only a single transmit antenna is made active at a particular instant of time. Thus the transmit vector has only one nonzero element. The information sequence is segregated into two streams namely, spatial bit selection stream and transmission bit stream. Here N_t represent the number of transmit antennas and M represent the modulation order. The first $\log_2 N_t$ bits determine the active antenna. These bits constitute the selection bit stream. Thus, the active antenna index serves as one of the information dimensions. The remaining $\log_2 M$ bits are communicated by the selected antenna. This approach gives the benefits of spectrally efficient transmission and avoidance of Inter Channel Interference (ICI) [3, 21]. Thus, in SM systems, the number of bits per channel use is quantified as

$$\eta_{SM} = (\log_2 N_t + \log_2 M) \quad (6)$$

3.2 Generalized SM (GNSM)

The major disadvantage of SM scheme is that spectral efficiency increases logarithmically with the number of transmit antennas and modulation order. To overcome this limitation, GNSM scheme ensures that two antennas are active at all time instants by transmitting same or different symbols [3]. The spectral efficiency of this scheme is described by,

$$\eta_{GNSM} = \log_2 \binom{N_t}{N_a} + \log_2(M) \quad (7)$$

In the above equation, N_a represents the number of active antennas which is two for a generalized case.

3.3 Variable Generalized SM (VGSM)

In VGSM scheme number of active antennas are variable which can take on values from 1 to N_t . If the number of selected antennas are more than one the same symbol is transmitted from all the active antennas. The number of possible antenna combinations and spectral efficiency for VGSM scheme are respectively given by [3],

$$\text{Number of antenna combinations} = \sum_{n=1}^{N_t} \binom{N_t}{n} = 2^{N_t} - 1 \quad (8)$$

$$\eta_{VGSM} = \lfloor \log_2(2^{N_t} - 1) \rfloor + \log_2(M) \quad (9)$$

3.4 Improved or Extended SM (ISM or EXSM)

In ISM scheme there is no restriction on the number of active antennas over a symbol duration. This value can be any number between 1 to N_t . This scheme differs from VGSM

as, in ISM different symbols are transmitted from the active antennas when more than one antennas are selected. The spectral efficiency for the ISM scheme is given by [4, 5],

$$\eta_{ISM} = N_t + \log_2(M) \tag{10}$$

3.5 Enhanced SM (ESM)

The ESM scheme is designed to make use of one or two active antennas at any instant of time. If one antenna is active, a higher order modulation scheme (assume QPSK) is employed. On the other hand, if two antennas are activated, a lower order modulation scheme (exactly half the constellation energy of the primary selected, here BPSK) is used. The spectral efficiency provided by this scheme is quantified as [6, 7],

$$\eta_{ESM} = \log_2\left(\frac{N_t}{N_a}\right) + \log_2(M) \tag{11}$$

3.6 Quadrature SM (QSM)

Mesleh et al. has proposed a scheme referred to as Quadrature Spatial Modulation (QSM) in which the spatial dimension is subdivided into in-phase and quadrature components. This scheme yields an improvement in spectral efficiency as compared with conventional SM. The spectral efficiency of the scheme is given by [8, 12, 13],

$$\eta_{QSM} = 2 \times \log_2 N_t + \log_2 M \tag{12}$$

4 Redesigned Spatial Modulation for Spatially Correlated Channels

The block schematic of the Redesigned Spatial Modulation (ReSM) system is shown in Fig. 1. This scheme has been designed to operate efficiently in SC environments. The performance of the scheme is identical to that of SM when employed under conditions of zero channel correlation. The underlying idea of ReSM explained with QPSK modulation scheme is illustrated in Table 1 and explained for 4 bpcu. The spectral efficiency can be enhanced to 6 bpcu using higher order modulation schemes. (Simulations and analyses are based on the table given in Appendix-II, for 6 bpcu). Here we have considered the distance between two elements of transmitter array to be TX separation, similarly RX separation is the distance between two elements of receiver array.

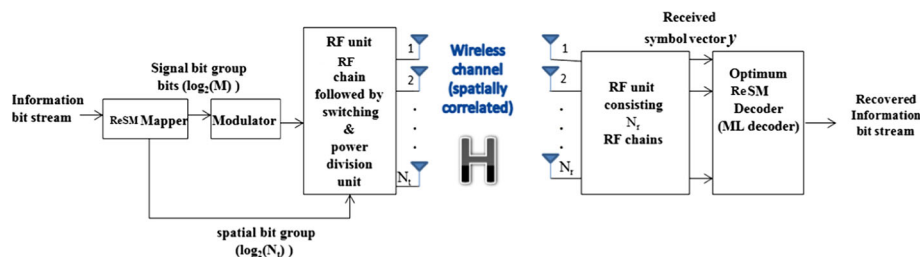
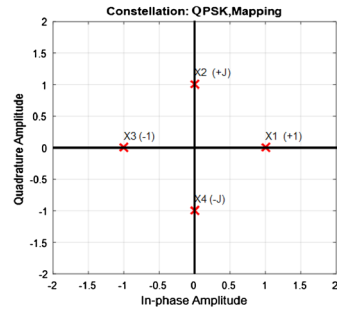


Fig. 1 Block diagram of the proposed Redesigned Spatial Modulation system

Table 1 Mapping followed in ReSM for 4 bpcu employing QPSK constellation

Possible groups of $\log_2 MN_t$ (4) bits /channel/use	TX 1	TX 2	TX 3	TX 4
0000	x_1	-	-	-
0001	x_2	-	-	-
0010	x_3	-	-	-
0011	x_4	-	-	-
0100	-	-	-	x_1
0101	-	-	-	x_2
0110	-	-	-	x_3
0111	-	-	-	x_4
1000	$x_1/\sqrt{2}$	$x_2/\sqrt{2}$	-	-
1001	$x_2/\sqrt{2}$	$x_3/\sqrt{2}$	-	-
1010	$x_3/\sqrt{2}$	$x_4/\sqrt{2}$	-	-
1011	$x_4/\sqrt{2}$	$x_1/\sqrt{2}$	-	-
1100	-	-	$x_1/\sqrt{2}$	$x_2/\sqrt{2}$
1101	-	-	$x_2/\sqrt{2}$	$x_3/\sqrt{2}$
1110	-	-	$x_3/\sqrt{2}$	$x_4/\sqrt{2}$
1111	-	-	$x_4/\sqrt{2}$	$x_1/\sqrt{2}$



It should be noted that TX1, TX2 are tightly correlated, TX1, TX3 are less correlated and TX1, TX4 are least correlated due to their mutual spacing, this is true for other groups as well. The mapping of signal constellation points to an antenna or antennas is solely based on the channel correlation values. Hence the given table is not static, instead it can be dynamically reassigned based on the channel conditions to improve the performance with an extra processing latency and feedback path. The assignment of different QPSK symbols $\{x_1, x_2, x_3, x_4\}$ to various possible four bit sequences is specified. We see that corresponding to the sequences $\{0000, 0001, 0010, 0011\}$, four distinct QPSK symbols are transmitted respectively from the 1st transmit antenna. The sequences $\{0100, 0101, 0110$ and $0111\}$ are communicated by transmitting four distinct QPSK symbols from transmit antenna number 4. Spatial separation between TX1 and TX4 is maximum and hence transmit channel 1 and transmit channel 4 are least correlated. This assignment of symbols to antennas is to facilitate easy identification of transmitting antenna at the receiver. Further a study of the Table 1. reveals that sequences $\{1000, 1001, 1010,$ and $1011\}$ are communicated by transmitting the adjacent QPSK symbols from antennas 1 and 2. Finally the sequences $\{1100, 1101, 1110$ and $1111\}$ are communicated by transmitting the adjacent QPSK symbols from antennas 3 and 4. This assignment is designed to yield maximum Signal to Noise Ratio (SNR) even when the signals received at the antennas are correlated due to small antenna spacing. The output is represented in the form of a vector as given below

$$\mathbf{y} = \sqrt{\rho}\mathbf{H}_c\mathbf{x} + \mathbf{n} \tag{13}$$

where $\mathbf{y} = [y_0 y_1 \dots y_{N_r}]^T$ indicates the received symbol vector of length $N_r \times 1$. Further, $\mathbf{x} \in \mathbf{X}$ denotes a transmitted symbol vector of length $N_t \times 1$, \mathbf{X} is the set of all possible transmit vectors for a given N_t and modulation order M . \mathbf{H}_c is a correlated channel matrix of dimension $N_r \times N_t$. The individual elements $h_{ij} \in \mathbf{H}_c$ denote the channel gain from j th transmit antenna to i th receive antenna. ρ represents the average SNR at each receive antenna. $\mathbf{n} = [n_1 n_2 \dots n_{N_r}]^T$ denotes the noise vector of length $N_r \times 1$. The complex entries of \mathbf{n} are assumed to be circularly symmetric, independent and identically Gaussian

distributed (i.i.d) with zero-mean and unit-variance. This distribution is represented by $(\mathcal{CN}(0, 1))$. GNSM, VGSM, ISM chooses antenna sets in the pattern given by

$$\eta = \binom{N_t}{1} + \binom{N_t}{2} + \dots + \binom{N_t}{N_t} \tag{14}$$

above three SM schemes does not impose any criteria for selecting the subsets. When spacing becomes dense i.e. the spacing between the antenna elements in transmit array is very small (correlated environment), gains of the individual channels obtained from adjacently placed transmit antennas are likely to be approximately equal as shown below

$$h_{rp} \sim h_{r+p}; \forall r \in \{1, 2, \dots, N_t\}, p \in \{1, 2, \dots, N_t\} \tag{15}$$

where h_{rp} represents channel gain from p th transmit antenna to r th receive antenna. As a consequence, there exists difficulty in determining the exact location of the transmit antenna that has radiated a given symbol at the receiving end. This leads to deterioration in the performance. In order to overcome the performance deterioration we have come up with a new strategy of antenna selection in ReSM. A brief description of antenna selection and detection for ReSM schemes is given in the following sections.

a. Methodology of antenna selection algorithm in ReSM:

The ReSM scheme has been designed to minimize possible ambiguities in antenna selection. This scheme achieves a spectral efficiency of $(\log_2 M + \log_2 N_t)$ bpcu. Unlike other variants of SM, every spatial bit group in ReSM corresponds to a unique transmit antenna subset that comprises of 1 or 2 active transmit antennas. Whenever two transmit antennas are active, the transmitted symbol amplitude is scaled by $1/\sqrt{2}$. This ensures that the average power per transmitted symbol is same. Every spatial bit group in ReSM is identified by a unique transmit antenna subset and modulation symbol or symbols. We see that N_t distinct transmit antenna subsets needs to be chosen amongst the available $\binom{N_t}{1} + \binom{N_t}{2}$ single and two element transmit antenna subsets. In the following paragraph, we have described the criteria used for choosing the transmit antenna subsets. Amongst $\binom{N_t}{1}$ single element subsets available, $\frac{N_t}{2}$ subsets are chosen such that the selected single transmit antenna is sufficiently apart from each other. The remaining $\frac{N_t}{2}$ subsets are selected from $\binom{N_t}{2}$ two element subsets. For $N_t = 4$, active antenna assignment is illustrated in Table 1. Antennas 1 and 4 (which has maximum spatial separation) are chosen when a single transmit antenna is selected for radiation. Antennas 2 and 3 will not be preferred for transmission to avoid ambiguity at the receiver due to correlation as explained above. The received symbol y_r for the single transmit antenna is given below

$$y_r = x_q h_{r1} + n_r, \forall r \in \{1, 2, \dots, N_r\} \tag{16}$$

$$y_r = x_q h_{r4} + n_r, \forall r \in \{1, 2, \dots, N_r\}. \tag{17}$$

Since the transmitting antenna can be identified distinctly by its AOA determination, there is no ambiguity about the transmitting antenna in this case. When two transmit antennas are active, the subsets chosen are either $\{1, 2\}$ or $\{3, 4\}$.

The received symbols in these cases are respectively specified by,

$$\begin{aligned}
 y_r &= \frac{x_q}{\sqrt{2}} h_{r1} + \frac{x_{q+1}}{\sqrt{2}} h_{r1} + n_r = \frac{1}{\sqrt{2}} (h_{r1}x_1 + h_{r1}x_2) + n_r, \forall r \in \{1, 2, \dots, N_r\} \\
 y_r &= \frac{x_q}{\sqrt{2}} h_{r1} + \frac{x_{q+1}}{\sqrt{2}} h_{r1} + n_r = \frac{1}{\sqrt{2}} (h_{r1}x_2 + h_{r1}x_3) + n_r, \forall r \in \{1, 2, \dots, N_r\} \\
 y_r &= \frac{x_q}{\sqrt{2}} h_{r1} + \frac{x_{q+1}}{\sqrt{2}} h_{r1} + n_r = \frac{1}{\sqrt{2}} (h_{r1}x_3 + h_{r1}x_4) + n_r, \forall r \in \{1, 2, \dots, N_r\} \\
 y_r &= \frac{x_q}{\sqrt{2}} h_{r1} + \frac{x_{q+1}}{\sqrt{2}} h_{r1} + n_r = \frac{1}{\sqrt{2}} (h_{r1}x_4 + h_{r1}x_1) + n_r, \forall r \in \{1, 2, \dots, N_r\} \\
 y_r &= \frac{x_q}{\sqrt{2}} h_{r3} + \frac{x_{q+1}}{\sqrt{2}} h_{r3} + n_r = \frac{1}{\sqrt{2}} (h_{r3}x_1 + h_{r3}x_2) + n_r, \forall r \in \{1, 2, \dots, N_r\} \\
 y_r &= \frac{x_q}{\sqrt{2}} h_{r3} + \frac{x_{q+1}}{\sqrt{2}} h_{r3} + n_r = \frac{1}{\sqrt{2}} (h_{r3}x_2 + h_{r3}x_3) + n_r, \forall r \in \{1, 2, \dots, N_r\} \\
 y_r &= \frac{x_q}{\sqrt{2}} h_{r3} + \frac{x_{q+1}}{\sqrt{2}} h_{r3} + n_r = \frac{1}{\sqrt{2}} (h_{r3}x_3 + h_{r3}x_4) + n_r, \forall r \in \{1, 2, \dots, N_r\} \\
 y_r &= \frac{x_q}{\sqrt{2}} h_{r3} + \frac{x_{q+1}}{\sqrt{2}} h_{r3} + n_r = \frac{1}{\sqrt{2}} (h_{r3}x_4 + h_{r3}x_1) + n_r, \forall r \in \{1, 2, \dots, N_r\}
 \end{aligned}
 \tag{18}$$

This scheme can be readily extended to higher modulation orders, antenna combinations and antenna requirement for all the modulation schemes as stated below in Tables 2 and 3.

Note: (Details of antenna selection for ReSM 6 bpcu is provided in Table 6 of Appendix-2).

b. Optimal maximum likelihood detection criterion:

Optimal Maximum Likelihood (ML) detection strategy for conventional SM as described by Jeganathan et al. [10] has been adopted for demodulation of SM and all its variants. The ML estimates are provided by

$$\hat{\mathbf{X}}_{ML} = \arg \min_{\mathbf{x} \in \mathcal{X}^m} \|\mathbf{y} - \mathbf{H}_c \mathbf{X}\|_F^2 \tag{19}$$

$$\hat{\mathbf{X}}_{ML} = [\hat{j}_{ML}, \hat{q}_{ML}] = \arg \min_{j,q} \sqrt{\rho} \|\mathbf{g}_{jq}\|_F^2 - 2\text{Re}\{\mathbf{y}^H \mathbf{g}_{jq}\} \tag{20}$$

where $\mathbf{g}_{jq} = \mathbf{h}_j x_q$, $1 \leq j \leq N_r$, $1 \leq q \leq M$, M is the modulation order \mathbf{y}^H is the Hermitian of \mathbf{y} . $\hat{j}_{ML}, \hat{q}_{ML}$ provides information about the estimated active transmit antenna index and the

Table 2 Transmit antenna selection

Number of transmit antennas (“ N_t ”) available	2	4	8
Number of bits mapped to spatial domain (“ $\log_2 N_t$ ”)	1	2	3
Enumeration of transmit antenna subsets chosen as per proposed ReSM scheme	{1}, {1,2}	{1},{4}, {1,2},{3,4}	{1} {3} {5} {7} {1,2} {3,4} {5,6} {7,8}

Table 3 Active antenna requirement

	SM	SMX	GNSM	VGSM	ISM or EXSM	ESM	QSM	ReSM (proposed)
Min	1	N_t	2	1	1	1	1	1
Max	1	N_t	N_t	N_t	N_t	2	2	2

radiated spatial signal constellation symbol respectively. The performance evaluation of the system is quantified using an analytical upper bound and Monte-Carlo simulations. ML decoder provides a significant enhancement in Bit Error Rate (BER) performance over sub-optimal MRRC detection method as showed in [10].

5 Analytical Treatment

To verify the accuracy of Monte Carlo simulations performed for the proposed ReSM and acquire a proper understanding into its characteristics under SC channels and measured indoor channel, bounds on the PEP are considered in this section. It is assumed that perfect channel state information (CSI) is available at the receiver and optimum ML decoding method is used. Following Younis et al. [3], the Average Pairwise Error Probability (APEP) can be found using the union bound [14, 16, 20] and ABER for the proposed ReSM system can be approximated by

$$ABER_{ReSM} \leq \frac{1}{2^\eta} \sum_{n_t, s_t} \sum_{n, s} \frac{N(x_{n_t, s_t}, x_{n, s})}{\eta} E_H\{PEP\} \tag{21}$$

In this equation, n_t is the number of active transmit antennas, s_t is the transmit symbol, η is the spectral efficiency, $N(x_{n_t, s_t}, x_{n, s})$ is the total number of bits in error between $x_{n_t, s_t}, x_{n, s}$, $E_H\{\cdot\}$ is the expectation across the channel matrix \mathbf{H} . The PEP is given by

$$PEP(x \rightarrow x') = P_r(\|y - H_c x_{n_t, s_t}\|^2 > \|y - H_c x_{n, s}\|^2 | \mathbf{H}) \tag{22}$$

$$= Q\left(\sqrt{\frac{\|H_c \zeta\|^2}{2\sigma_n^2}}\right) \tag{23}$$

here $\zeta = x_{n_t, s_t} - x_{n, s}$. Taking the expectation, PEP can be simplified as

$$PEP(x \rightarrow x') \leq \frac{1}{2\pi} \frac{\exp(-\frac{1}{4\sigma_n^2} \text{vec}(\tilde{\mathbf{H}}^H) \hat{\Gamma} (\mathbf{I}_{N_r N_t} + \frac{1}{4\sigma_n^2} \mathcal{L}_H \hat{\Gamma})^{-1} \text{vec}(\tilde{\mathbf{H}}^H))}{\left| \mathbf{I}_{N_r N_t} + \frac{1}{4\sigma_n^2} \mathcal{L}_H \hat{\Gamma} \right|} \tag{24}$$

where $\hat{\Gamma} = R_{REC} \otimes (\zeta \zeta^H R_{TRAN})$, \mathcal{L}_H is the covariance matrix, $\tilde{\mathbf{H}}$ is the mean matrix, \otimes is the Kronecker product and $(\cdot)^H$ is the Hermitian. $\text{vec}(\mathbf{H})$ is the column of matrix \mathbf{H} into a column vector, \mathbf{I}_n is an $n \times n$ identity matrix.

The channel matrix \mathbf{H} is contrived similar to the one explained in [20, 21]. This allows the behavior of the channel to be identical to that of the standard 3GPP model for SC fading channels. The mean matrix and the covariance matrix are entirely dependent on the type of the channel used and the channel matrix for different fading scenarios. It is given as follows:

Equation (24) is an upper bound for both Rayleigh fading as well as Rician fading as indicated in [3].

The mean matrix $\check{\mathbf{H}} = \mathbf{0}_{N_r \times N_t}$, the covariance matrix $\mathcal{L}_H = \mathbf{I}_{N_r N_t}$ holds good for Rayleigh fading conditions [3].

$$\text{For Rician fading mean matrix is defined as } \check{\mathbf{H}} = \sqrt{\frac{K}{1+K}} \times \mathbf{1}_{N_r \times N_t} \text{ and} \tag{25}$$

$$\text{Covariance matrix is given as } \mathcal{L}_H = \sqrt{\frac{1}{1+K}} \times \mathbf{I}_{N_r N_t} \tag{26}$$

K represents the Rician factor. $K = 3(5\text{dB})$.

In Sect. 7, the bound in Eq. (24) is shown to be an upper bound for the proposed ReSM scheme (as part of the simulation). Proof of Eq. (24) is shown in Appendix 1.

6 Receiver Computational Complexity Comparison

In this section, the receiver complexity of ReSM-ML is compared with all other conventional SM schemes for the same spectral efficiency. The spectral efficiency of all the systems under comparison is specified by Eqs. (6–12). Following Younis et al. [3] the computational complexity of SM-ML is given as,

$$C_{\text{SM-ML}} = 8N_r 2^{\eta}_{\text{SM}} \tag{27}$$

where the ML detector searches through the whole search space.

The computational complexity of GNSM-ML and VGSM-ML are identical [3]. The result is reproduced here for convenience and comparison.

$$\begin{aligned} C_{\text{GNSM-ML}} &= 6N_r 2^{\eta}_{\text{GNSM}} \\ C_{\text{VGSM-ML}} &= 6N_r 2^{\eta}_{\text{VGSM}}, \text{ thus we see that} \\ C_{\text{GNSM-ML}} &= C_{\text{VGSM-ML}} \end{aligned} \tag{28}$$

In the following paragraph, we have computed the computational complexity of ISM/EXSM systems.

Let us consider an ISM system with $N_t = 4, N_r = 4, \eta = 6$ bpcu. Since these systems are characterized by $\eta = 6$ bpcu, the total number of available antenna combinations are 64. There are $\binom{4}{1} \times 4$ possible single antenna combinations and $\left(\binom{4}{2} \times 4\right) \times 2$ two antenna combinations. Different symbols can be transmitted from multiple activated antennas. When only one antenna is active, the transmit antenna can transmit one out of the four possible symbols based on the input bit pattern hence $N_t \times M$ possible combinations exist. The remaining combinations numbering $2^{\eta} - 2^{\log_2(N_t \times M)}$ are accomplished through two active antenna arrangements.

For single active antenna combination, the complexity of the system is given by

$$C_{\text{ISM-ML}(1)} = 8N_r 2^{\log_2(N_t \times M)} \tag{29}$$

For two active antenna combinations, the complexity of the system is given by

$$C_{\text{ISM-ML}(2)} = 12N_r(2^\eta - 2^{\log_2(N_t \times M)}) \tag{30}$$

The maximum number of computational steps required per transmitted symbol is

$$C_{\text{ISM-ML}} = 12N_r(2^\eta - 2^{\log_2(N_t \times M)}) \tag{31}$$

Further, for QSM systems the complexity of QSM-ML scheme as given in [13] is quantified by

$$C_{\text{QSM-ML}} = 8N_r 2^\eta \tag{32}$$

Following [7], where the complexity of ESM-ML scheme was computed taking into account the presence of only one receive antenna is given by

$$C_{\text{ESM-ML}} \leq C_{\text{SM-ML}} \tag{33}$$

We will now determine the receiver computational complexity of the proposed ReSM scheme. Consider the above example for $N_t = 4, N_r = 4, \eta = 6$ bpcu and $M = 16$ QAM, symbol to antenna mapping is explained in Appendix-2. Let us determine the number of computations required to estimate $|Y - H\hat{X}|^2$ where \mathbf{H} is the $N_r \times N_t$ complex channel matrix, \hat{X} is the $N_t \times 1$ complex transmitted matrix, $Y - H\hat{X}$ is the $N_r \times 1$ complex received matrix, multiplication of \mathbf{H} by \hat{X} requires N_t complex multiplications. Each complex multiplication in turn requires four real multiplications. Therefore each row give rise to $4 \cdot N_t$ real multiplications.

Since \mathbf{H} has N_r rows, total number of real multiplications required to evaluate $\mathbf{H}\hat{X}$ is given by $4 \cdot N_t \cdot N_r$.

$$|Y - H\hat{X}|^2 = (Y - H\hat{X})^H (Y - H\hat{X}) \tag{34}$$

Here total number of multiplications (real) involved in computing $|Y - H\hat{X}|^2$ is equal to $4(N_t + 1)N_r$. The above analysis is for one transmit vector \hat{X} . There exists 2^η possible combinations of vector \hat{X} . Therefore total computational complexity is $4(N_t + 1)N_r \times 2^\eta$. First $\binom{16}{1}$ symbols are transmitted through the transmitting antenna 1 and the same symbols are transmitted through transmitting antenna 4, constituting to the total of $\binom{16}{1} \times 2$ combinations. Therefore the computational complexity of ReSM-ML detector for single active antenna combination is given by $8N_r 2^{\eta-1}$. For two active transmit antennas, transmitting antenna 1 and 2 combined has $\binom{16}{1}$ combinations and the next $\binom{16}{1}$ combinations are pervaded by antennas 3 and 4. Hence the computational complexity when transmitting two different symbols from two antennas can then be written as $12N_r 2^{\eta-1}$. Apparently all combinations of single active and two active antenna constitutes

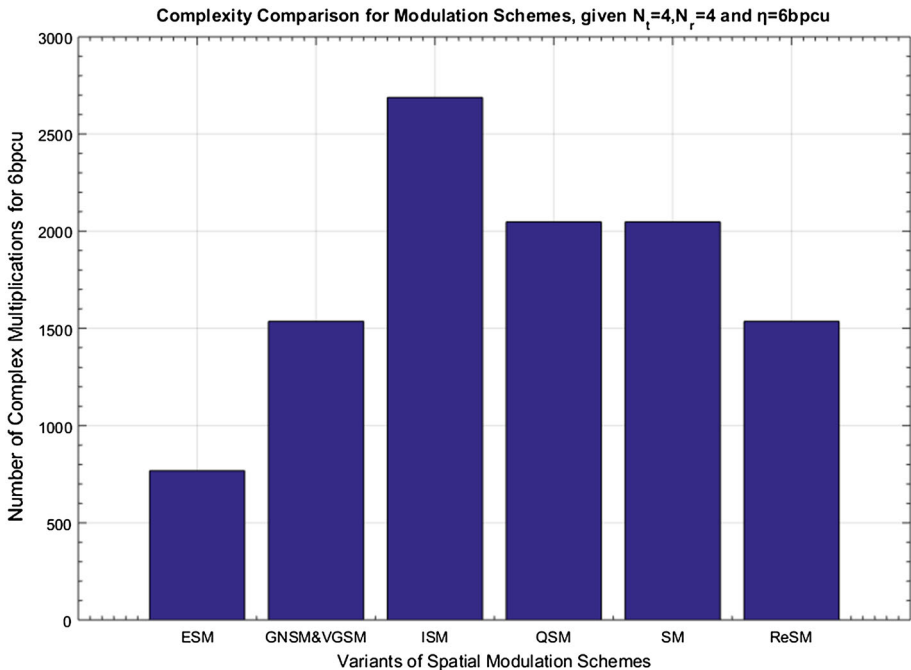


Fig. 2 Complexity comparison

to total of 64 groupings. The maximum number of computational steps required per transmitted symbol is shown in (35) and plotted in Fig. 2.

$$C_{\text{ReSM}} = 12N_r 2^{\eta-1} \quad (35)$$

7 Simulation Results

This subsection is devoted to a description of the performance of ReSM and the comparison of these results with conventional SM under various channel conditions. Monte Carlo simulations have been carried out with a minimum of 10^6 channel realizations. The ABER values are plotted against SNR. A Rician K factor equal to 3 has been assumed in all simulations pertaining to the Rician fading environment. As per 3GPP standards, channel correlation is observed when antenna separation is 0.1λ at the transmitter and 0.5λ at the receiver. These results specify the performance obtained under 4G/LTE channel scenario as per 3GPP standards [15]. Further, we witness denser correlation environment when antenna separation at the receiver reduces to 0.1λ . The performance of all variants of SM (SM, GNSM, VGSM, ISM/EXSM, ESM, QSM and TCSM) have been compared against ReSM under conditions of equal spectral efficiency (4 bpsu and 6 bpsu). Later, to determine typical channel coefficients for indoor communication, a 2×2 MIMO system was set up in the laboratory using USRP B210. The channel coefficients obtained by these measurements correspond to Rician fading in the presence of spatial correlation brought about by close antenna spacing. Our study indicates that ReSM scheme provides an

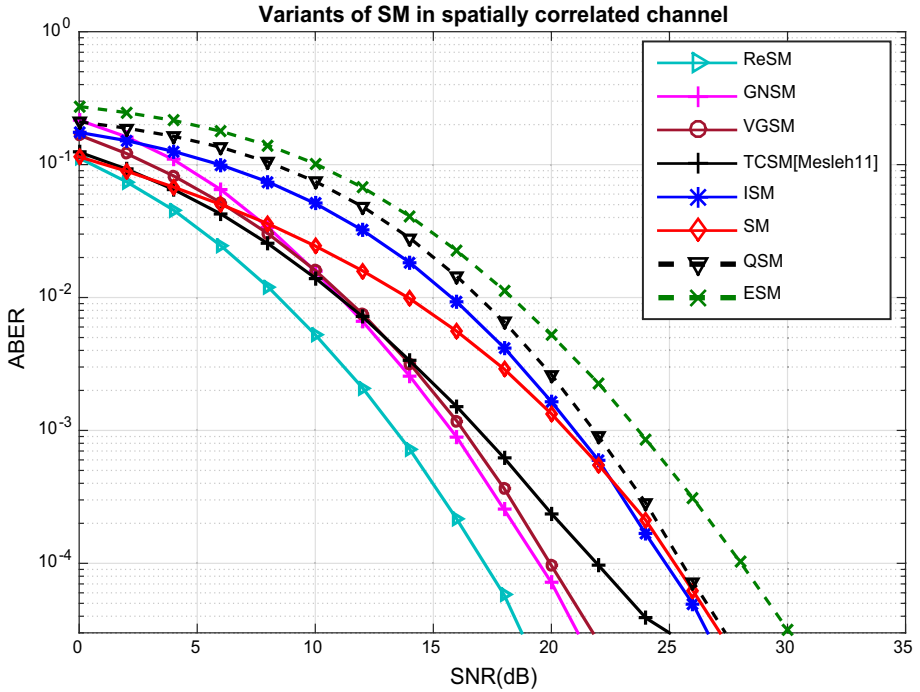


Fig. 3 BER performance of 4×4 systems with TX separation = 0.1λ and RX separation = 0.5λ yielding $\eta = 6$ bpcu spectral efficiency, in a SC channel

improvement of approximately 7 dB over conventional SM system in indoor environment with antenna spacing of 0.1λ at the transmitter and 0.5λ at the receiver.

In Fig. 3, it is seen that ReSM outperforms all the other variants of SM. The environment under consideration is the typical mobile scenario with 3GPP specification designed for 4G/LTE [15]. The transmitter separation (TX separation) of 0.1λ and receiver separation (RX separation) of 0.5λ . These comparisons have been carried out at ABER of 10^{-4} . ReSM offers a performance improvement over GNSM, VGSM schemes by ~ 3 dB, TCSM [9, 11] by ~ 5 dB, and almost 7 dB over ISM, SM, QSM systems and an improvement of about ~ 10 dB in comparison with ESM systems.

A smaller change in the antenna separation at the receiver (RX separation = 0.3λ) causes change in performance of all the competing schemes due to higher spatial correlation. This is documented in Fig. 4. We observe that even under these changed conditions, the performance of ReSM is superior to all the other schemes. ReSM offers a performance improvement over ISM, QSM, TCSM schemes by ~ 0.5 dB in higher SNR regime, ~ 3.4 dB over GNSM, VGSM and an improvement of ~ 10 dB over SM system.

In Fig. 5, it is seen that a further reduction in the receiver antenna spacing (RX separation = 0.1λ) leads to dense spatial correlation resulting a significant change in performance of all the SM schemes. The comparison in Fig. 5 shows that ReSM outperforms by ~ 2 dB, 2.5dB, 3.5dB, 3.6dB, 9dB, 11dB over TCSM, VGSM, GNSM, SM, QSM and ESM schemes respectively.

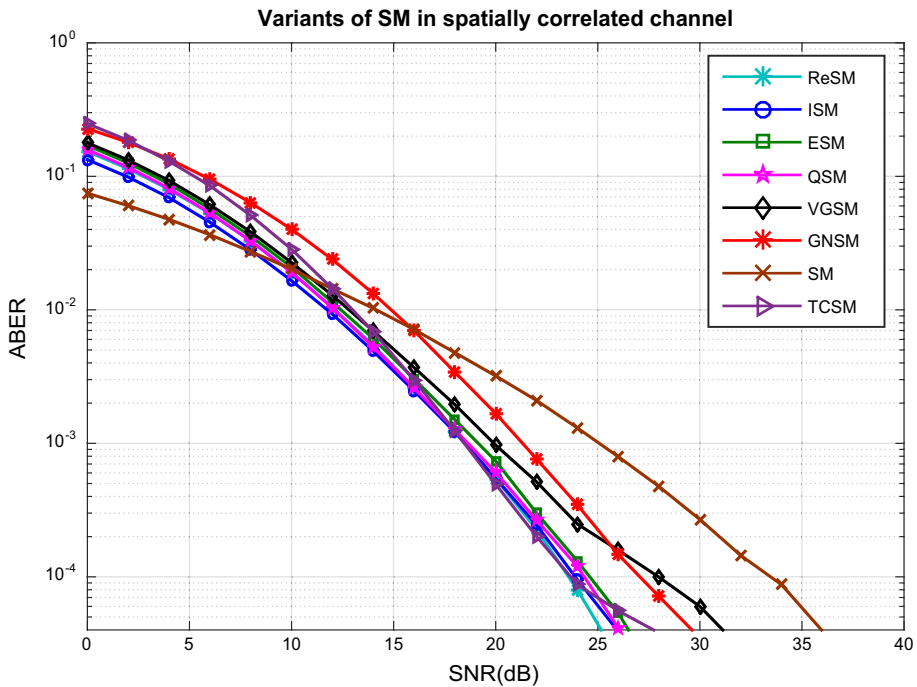


Fig. 4 BER performance of 4×4 systems with TX separation = 0.1λ and RX separation = 0.3λ yielding $\eta = 6$ bpcu spectral efficiency, in a SC channel

It has been observed that some configurations for 2×4 systems which produces a spectral efficiency of $\eta = 4$ bpcu cannot be constructed because of its impediments in choosing constellation points and antenna groupings. From Fig. 6, it is seen that for dense spatial correlated channel conditions ReSM offers a performance improvement of $\sim 1\text{dB}, 2\text{dB}, 2\text{dB}, 2.5\text{dB}$ over VGSM, GNSM, ISM and SM schemes respectively.

Figure 7 illustrates the relative performance of 4×4 systems yielding $\eta = 6$ bpcu in a Rician fading channel with $K = 3$. We see that the performance of ReSM is superior to SM, TCSCM schemes by about $\sim 2\text{dB}$. The $\sim 0.8\text{dB}$ advantage associated with VGSM and QSM arises from the fact that both antennas in VGSM are transmitting the same symbol and QSM uses lower order modulation scheme. This makes antenna identification easier and minimizes the errors arising from antenna misidentification in strong LOS environment. We also see that the plots corresponding to ReSM and VGSM converge at SNR value of 20dB .

ABEP of the ReSM scheme is mathematically analyzed for MIMO configuration involving 4×4 system producing 6 bpcu. The performance of ReSM according to (24) has been compared with the performance obtained under Monte Carlo simulations, this has been demonstrated in Fig. 8. Close correspondence between the two plots is observed.

7.1 A Detailed Procedure for Channel Estimation Using USRP B210

To determine typical channel coefficients for indoor communication, a 2×2 MIMO system was set up in the laboratory by using USRP B210. It has an inbuilt RF frontend and

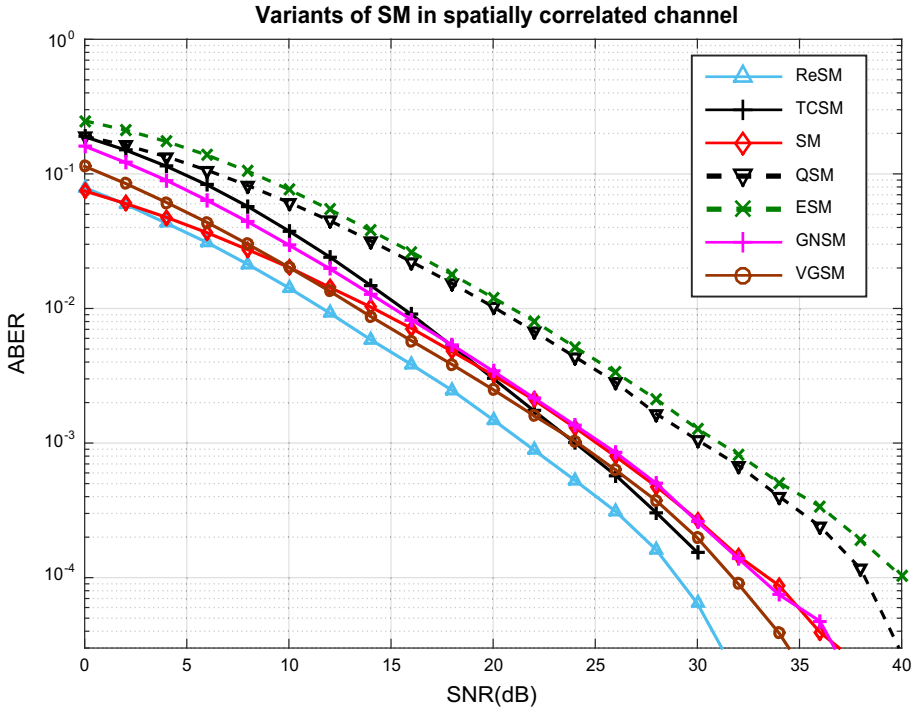


Fig. 5 BER performance of 4×4 systems with TX separation = 0.1λ and RX separation = 0.1λ yielding $\eta = 6$ bpcu spectral efficiency, in a SC channel

open reprogrammable FPGA that controls signal processing and other applications. The specifications of USRP B210 are shown in Table 4.

For an indoor environment, the minimum channel coherence time is measured to be approximately 20 ms as given in [18]. It's an unavoidable need to carry out the estimation of channel gains corresponding to all transmit antennas within a time period, which is lesser than the channel coherence time. To estimate the channel coefficients individually from the respective transmit antennas, we have made use of a transmit frame length comprising of 690 symbols. The 160 symbols out of 690 are used for frame synchronization and the rest 512 symbols (pilot symbols) are used to estimate the channel behavior. Peak detection technique is employed to achieve synchronization [3]. For synchronization, a sequence of 16 pulses with maximum power each separated by 9 zeros is used. The total of 512 symbols in the transmit frame of which first 256 symbols constitute to pilot 1 are transmitted from first active transmit antenna, during this period the second transmit antenna is deactivated. Similarly the rest 256 symbols constituting to pilot 2 are transmitted from second active transmit antenna while the first antenna is switched off. In order to distinguish between two frames 18 zero valued symbols are padded at the start of every frame. Most challenging aspect of this hardware realization is to have maximum SNR with minimum ISI (Inter symbol Interference). Upsampling and pulse shaping (matched filtering) are employed to achieve these two essential requirements. Every frame is sampled with an upsampling ratio of 2 and it is passed through a root raised cosine (RRC) filter with 32 taps and an excess bandwidth factor of at least 0.35. This process is

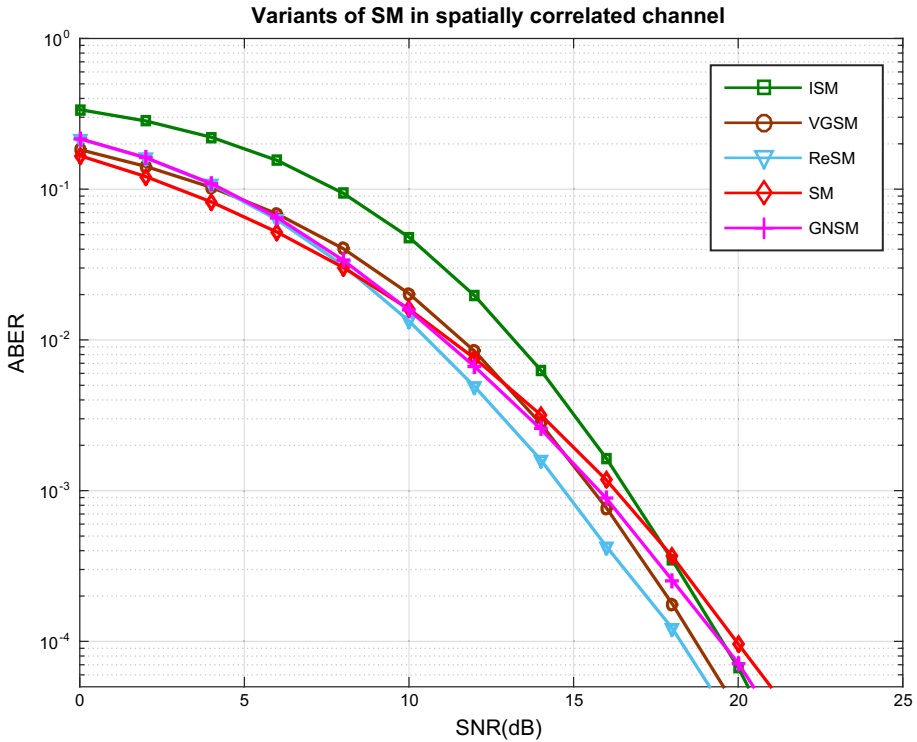


Fig. 6 BER performance of 2×4 systems with TX separation = 0.1λ and RX separation = 0.1λ yielding $\eta = 4$ bpcu spectral efficiency, in a SC channel

accomplished by the use of GNU radio software framework. In Fig. 9, we have demonstrated the transmit frame structure for USRP B210 which is used to estimate the channel coefficients.

In co-ordinance with the transmitting end, at the receiver, every received frame in baseband is appropriately down sampled and later passed through RRC filter having the same specifications.

For every filtered frame that is received, the receiver peaks are searched, this is done by considering certain threshold which in this case is 70% of the maximum value of the received vector. The received vector is allowed for further evaluation only if the number of peaks found to be 16 each followed by 9 zeros. The received pilot symbols arriving after the peak detection are used for channel estimation and the respective channel gains $h_{11}, h_{12}, h_{21}, h_{22}$ are evaluated using Least Square channel (LS) estimation principle.

Pilot 1 is used to estimate the channel gains h_{11}, h_{21} where h_{11} is the channel coefficient for receive antenna 1 from transmit antenna 1 and h_{21} is the channel coefficient for receive antenna 2 from transmit antenna 1. Similarly pilot 2 is used to estimate channel gains pertaining to h_{12}, h_{22} .

The spatial correlation of two transmit/receive antennas in an indoor laboratory environment has been analyzed in the presence of local scatterers and by varying the mutual distance between the two transmit antennas as well as receive antennas. Three set of channel measurements have been performed for distance of separation $\lambda, 0.5\lambda$ and 0.1λ between transmit array/receive array. The operating frequency is selected as 2 GHz,

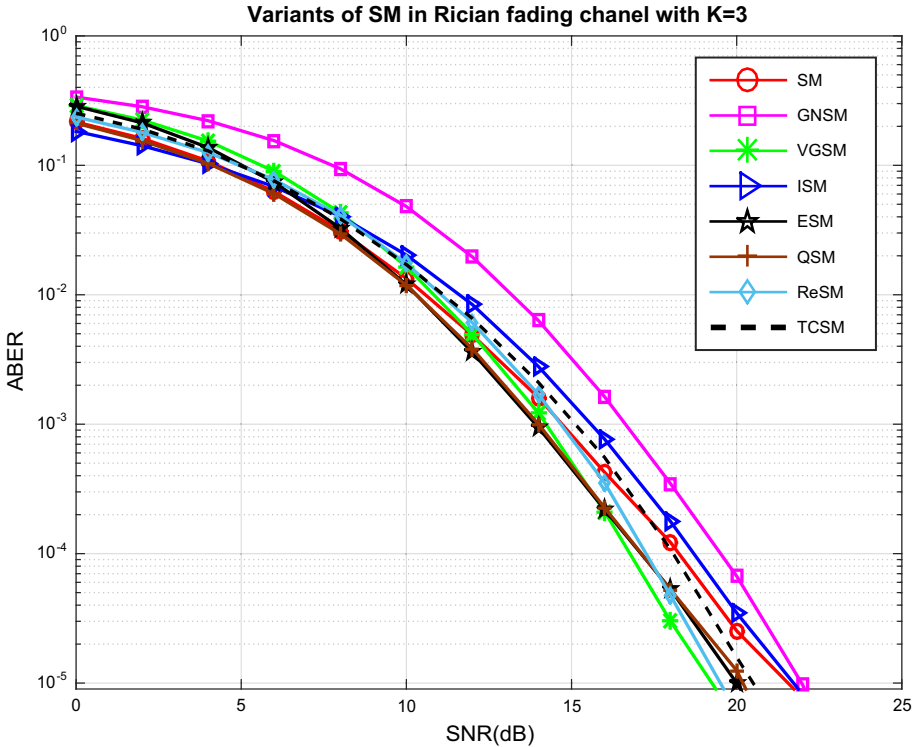


Fig. 7 BER performance of 4×4 systems yielding $\eta = 6$ bpcu spectral efficiency, in a Rician fading channel with $K = 3$

corresponding to it the antenna separations are $1\lambda = 15\text{cm}$, $0.5\lambda = 7.5\text{cm}$ and $0.1\lambda = 1.5\text{cm}$. To estimate the channel coefficients $h_{11}, h_{12}, h_{21}, h_{22}$ approximately 10^7 samples were processed.

The channel correlation values for the TX1 and TX2 are computed using the relation given below.

$$h_{mag_{ratio}}(n) = |h_{11}(n)|/|h_{12}(n)|; \quad \forall n$$

$$h_{angle_{diff}}(n) = \angle(h_{11}(n)) - \angle(h_{12}(n)); \quad \forall n$$

where $|h|$ represents magnitude of $h(n)$ and $\angle(h)$ represents phase value of h , n represents discrete time instance. Figures 10 and 11 shows the histograms of $h_{mag_{ratio}}$ values and $h_{angle_{diff}}$ values computed for antenna separations of $1\lambda, 0.5\lambda$ and 0.1λ respectively. Figure 10 shows, the histogram of the magnitude plot for different values of λ . It is observed that as the element separation of transmit array are reduced to 0.1λ , the histogram peak shift towards 1 showing a close correlation between TX1 and TX2. Similarly from Fig. 11, it is clear that the histogram peak of angular plot tend towards 0 as the antenna distance decreases. This indicates that lesser the antenna separation closer are the values of channel coefficients.

Figure 12, shows the close resemblance between Rician distribution and measured indoor environment in terms of PDF and CDF plots. This proves that the laboratory set up for a 2×2 MIMO system is a demonstration of Rician fading channel.

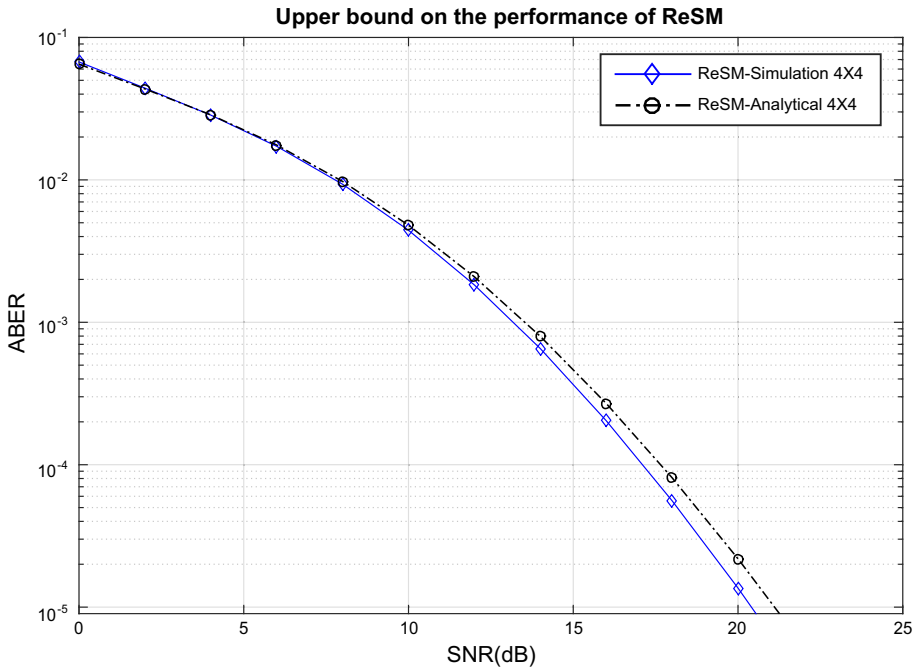


Fig. 8 BER performance of 4×4 systems with TX separation = 0.1λ and RX separation = 0.5λ yielding $\eta = 6$ bpcu spectral efficiency, in a SC channel

Table 4 USRP B210 specifications

RF coverage	70 MHz to 6 GHz
ADC/DAC	12 bit with a maximum sampling rate of 61.44MS/s
FPGA	Xilinx Spartan 6 XC6SLX150
MIMO capability	2×2 fully coherent
Supported bandwidths	56 MHz of instantaneous Bandwidth for 1×1 , and 30.72 MHz for 2×2
RF power output	>10 dBm (single channel)
Receive noise figure	<8 dB
Application peripheral interface (APIs)	GNU Radio, C++, Python

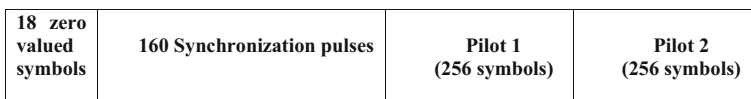


Fig. 9 Transmit frame structure used for channel estimation

Figure 13, shows the setup used in the laboratory to determine the values of channel coefficients from USRP B210 (2×2 MIMO). Figure 14, quantifies the performance of ReSM and SM for indoor environment with transmit antenna spacing of 0.1λ and receive

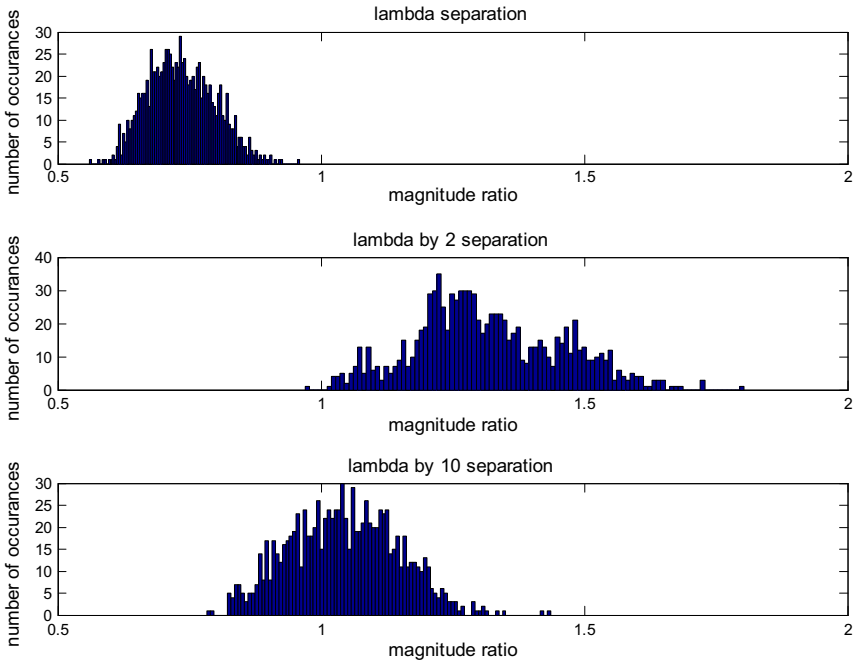


Fig. 10 Histograms of $h_{mag_{ratio}}$ values computed for transmit/receive antenna separation of 1λ , 0.5λ and 0.1λ

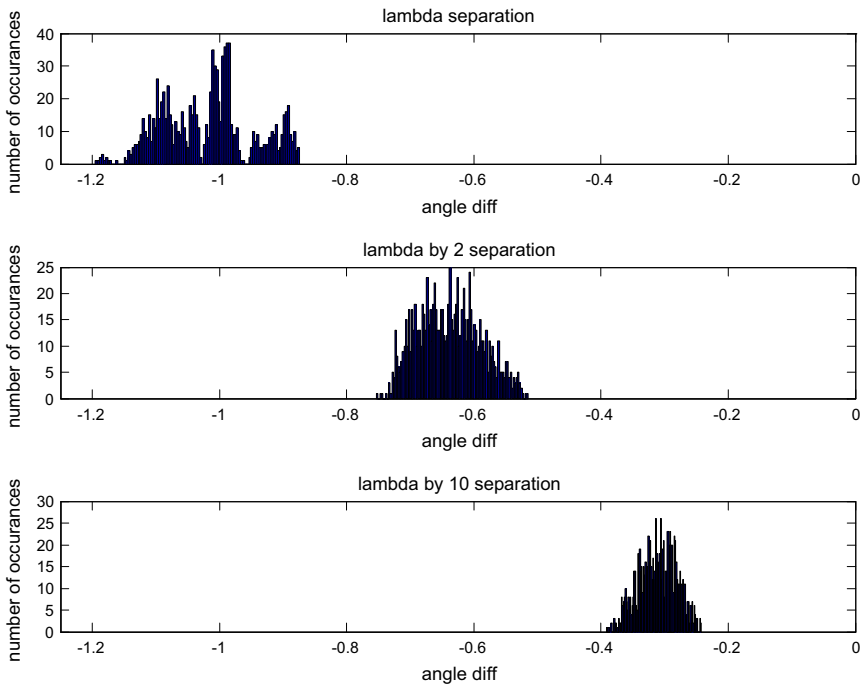


Fig. 11 Histograms of $h_{angle_{diff}}$ values computed for transmit/receive antenna separation of 1λ , 0.5λ and 0.1λ

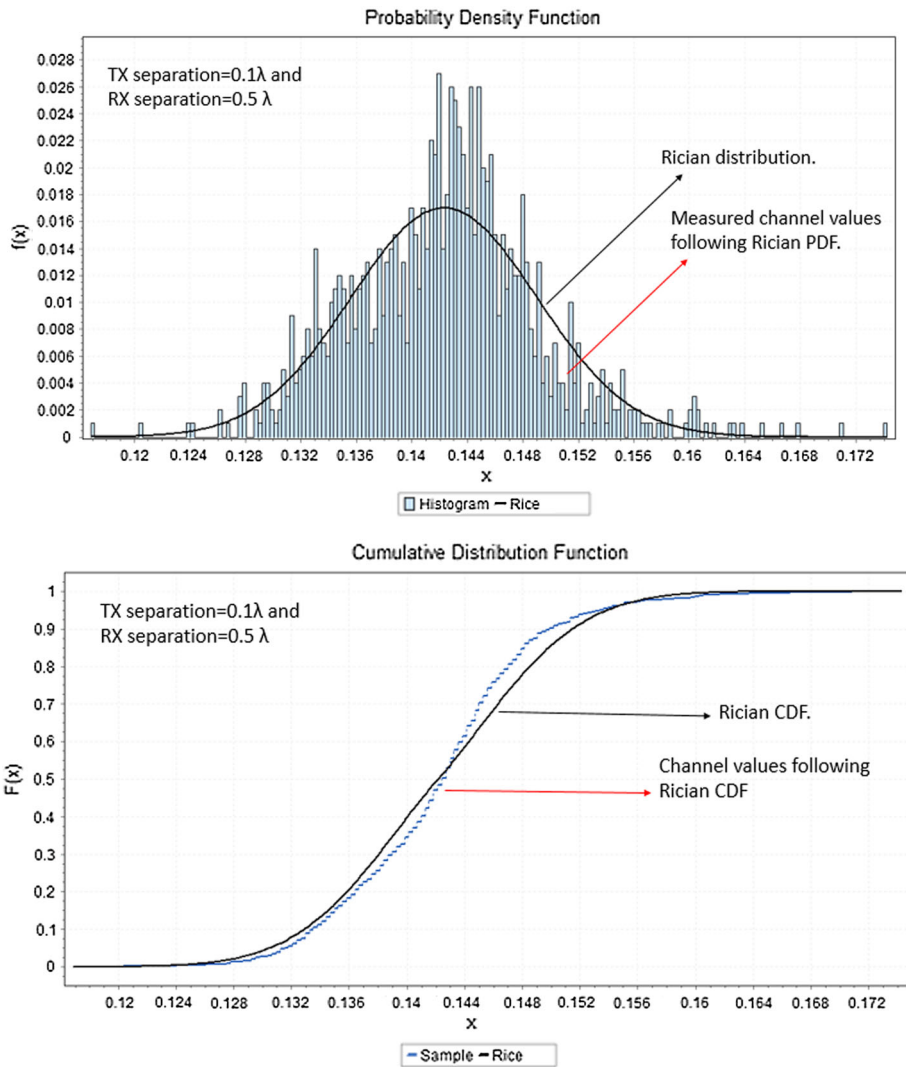


Fig. 12 Comparison of PDF-CDF between Rician and measured indoor channel with TX separation = 0.1λ , RX separation = 0.5λ

antenna spacing of 0.5λ (TX-RX separation is 3 meters). It is seen that ReSM scheme outperforms SM by approximately 7dB. A comparison of results is specified in Table 5. It is evident from the simulation plots that ReSM offers superior performance as compared to all the other competing schemes specifically in spatial correlated channel conditions.

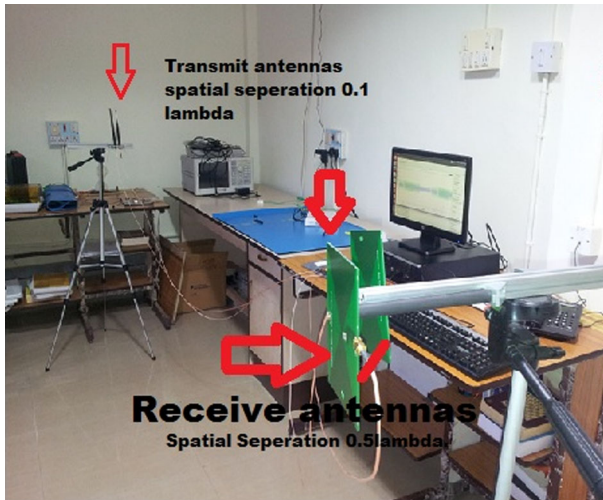


Fig. 13 Real measurements of 2×2 MIMO systems with a total distance TX-RX separation of 3 meters TX separation = 0.1λ and RX separation = 0.5λ yielding $\eta = 4$ bpcu spectral efficiency operating in an indoor environment

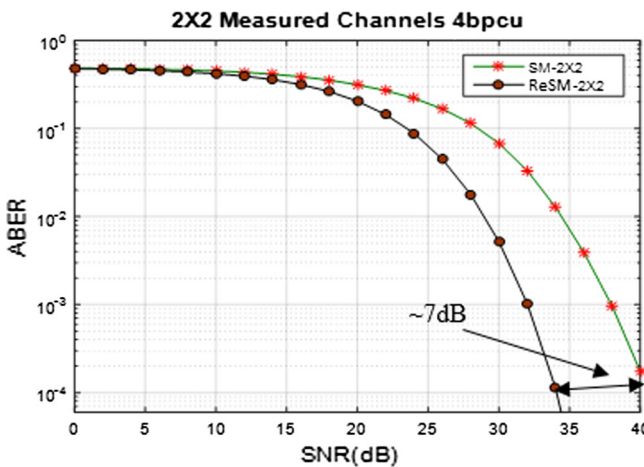


Fig. 14 Performance results of SM 2×2 and ReSM 2×2 with SC channel with channel coefficients obtained by USRP B210 at TX-RX separation of 3 meters. TX separation = 0.1λ , RX separation = 0.5λ yielding $\eta = 4$ bpcu

8 Conclusion

ReSM is a novel scheme designed to support reliable communication in SC channels exhibiting flat fading. The major advantage of ReSM is the absence of complex encoder/decoder when compared with TCSCM, it also provides BER advantage of ~ 4 dB. Additionally, a minimum of 3dB BER improvement is also observed over all other SM variants. The only exception is seen in Rician fading environment where VGSM gives a small performance improvement of ~ 0.5 dB over ReSM for $\eta = 6$ bpcu. These performance

Table 5 Performance comparison of ReSM with variants of SM, TCSM in SC and Rician fading channels

MIMO scheme	N_t, N_r	Spectral efficiency in bpcu	Required SNR at an ABER of 10^{-4} in dB
ReSM (SC)	4,4	6	~17
TCSM (SC)	4,4	6	~21 [11]
GNSM (SC)	4,4	6	~20
VGSM (SC)	4,4	6	~20
ISM(SC)	4,4	6	~24
SM (SC)	4,4	6	~24
ESM(SC)	4,4	6	~27
QSM (SC)	4,4	6	~26
ReSM (Rice K = 3)	4,4	6	~17.1
TCSM (Rice K = 3)	4,4	6	~19 [11]

The Bold characters indicates the results of the proposed work, as a comparison to the other existing works

gains are obtained without any additional burden of computational complexity. The ABER values obtained by exact closed form computations were compared with Monte-Carlo simulations and similarity between them was observed. Further, a typical real time indoor channel environment was set up using USRP B210 and channel measurements were carried out. This data was used to evaluate the performance of ReSM and SM schemes for indoor environments and ReSM outperforms conventional SM by ~7dB. Therefore, ReSM scheme can be advantageously employed in portable handheld devices, where antenna spacing is a major issue and battery power is limited.

Appendix 1

Proof of Eq. (24)

$$ABER_{ReSM} \leq \frac{1}{2^\eta} \sum_{n_t, s_t} \sum_{n_s} \frac{N(x_{n_t, s_t}, x_{n_s})}{\eta} E_H\{PEP\} \tag{36}$$

In this equation, n_t is the active transmit antenna, s_t is the transmit symbol, η is the spectral efficiency. $N(x_{n_t, s_t}, x_{n_s})$ is the total number of bits in error between x_{n_t, s_t}, x_{n_s} . $E_H\{\cdot\}$ is the expectation across the channel matrix H .

PEP is given by

$$PEP(x \rightarrow x') = P_r(\|y - H_C x_{n_t, s_t}\|^2 > \|y - H_C x_{n_s}\|^2 | H) = Q\left(\sqrt{\frac{\|H_C z\|^2}{2\sigma_n^2}}\right) = \frac{1}{\pi} \int_0^{\frac{\pi}{2}} \exp\left(-\frac{\|H_C z\|^2}{4\sigma_n^2 \sin^2(\theta)}\right) d\theta \tag{37}$$

where $z = x_{n_t, s_t} - x_{n_s}$

Following from [3] an alternative integral expression of the Q-function and taking the expectation of Eq. (37) we arrive at

$$E_H\{PEP\} = \frac{1}{\pi} \int_0^{\frac{\pi}{2}} \varphi\left(-\frac{1}{4\sigma_n^2 \sin^2(\theta)}\right) d\theta \tag{38}$$

where $\varphi(\cdot)$ is the moment generating function (MGF) of the random variable $\|H_c z\|^2$. From [3] it is clear that any i.i.d. Gaussian random variable with mean \check{v} and any Hermitian matrix \check{b} . The MGF then can be written as

$$\varphi(s) = \frac{\exp(s\check{v}^H \check{b} (I - s\mathcal{L}_v \check{b})^{-1} \check{v})}{|I - s\mathcal{L}_v \check{b}|} \tag{39}$$

\mathcal{L}_v is the covariance matrix of v . From (38) invoking MGF of $\|H_c z\|^2$ we can write

$$\varphi(s) = \frac{\exp(s \times \text{vec}(\check{H}^H) \hat{\Gamma} (I_{N_r N_t} - s\mathcal{L}_H \hat{\Gamma})^{-1} \text{vec}(\check{H}^H))}{|I - s\mathcal{L}_H \hat{\Gamma}|} \tag{40}$$

I_n is an $n \times n$ identity matrix, $\text{vec}(\mathbf{H})$ is the column of matrix \mathbf{H} into a column vector. $\hat{\Gamma} = R_{REC} \otimes (\mathcal{Z}^H R_{TRAN})$, \mathcal{L}_H is the covariance matrix, \check{H} is the mean matrix, \otimes is the Kronecker product and $(\cdot)^H$ is the Hermitian.

Making use of the Chernoff bound, PEP then can be written as,

$$PEP(x \rightarrow x') = \frac{1}{\pi} \int_0^{\frac{\pi}{2}} \frac{\exp\left(-\frac{1}{4\sigma_n^2 \sin^2(\theta)} \text{vec}(\check{H}^H) \hat{\Gamma} \left(I_{N_r N_t} + \frac{1}{4\sigma_n^2 \sin^2(\theta)} \mathcal{L}_H \hat{\Gamma}\right)^{-1} \text{vec}(\check{H}^H)\right)}{\left|I_{N_r N_t} + \frac{1}{4\sigma_n^2 \sin^2(\theta)} \mathcal{L}_H \hat{\Gamma}\right|} d\theta \tag{41}$$

Finally the upper bound is given by

$$ABER_{ReSM} \leq \frac{1}{2\eta} \sum_{n_t s_t} \sum_{n_s} \frac{N(x_{n_t s_t}, x_{n_s})}{\eta} \times \frac{1}{2\pi} \frac{\exp\left(-\frac{1}{4\sigma_n^2} \text{vec}(\check{H}^H) \hat{\Gamma} \left(I_{N_r N_t} + \frac{1}{4\sigma_n^2} \mathcal{L}_H \hat{\Gamma}\right)^{-1} \text{vec}(\check{H}^H)\right)}{\left|I_{N_r N_t} + \frac{1}{4\sigma_n^2} \mathcal{L}_H \hat{\Gamma}\right|} \tag{42}$$

Appendix 2

See Table 6.

Table 6 Mapping followed in ReSM for 6 bpcu employing 16QAM Constellation

Possible groups of $\log_2 MN_i(6)$ bits/channel/use	$Tx1$	$Tx2$	$Tx3$	$Tx4$
000000	x_1	–	–	–
000001	x_2	–	–	–
000010	x_3	–	–	–
000011	x_4	–	–	–
000100	x_5	–	–	–
000101	x_6	–	–	–
000110	x_7	–	–	–
000111	x_8	–	–	–
001000	x_9	–	–	–

Table 6 continued

Possible groups of $\log_2 MN_i(6)$ bits/channel/use	$Tx1$	$Tx2$	$Tx3$	$Tx4$
001001	x_{10}	—	—	—
001010	x_{11}	—	—	—
001011	x_{12}	—	—	—
001100	x_{13}	—	—	—
001101	x_{14}	—	—	—
001110	x_{15}	—	—	—
001111	x_{16}	—	—	—
010000	—	—	—	x_1
010001	—	—	—	x_2
010010	—	—	—	x_3
010011	—	—	—	x_4
010100	—	—	—	x_5
010101	—	—	—	x_6
010110	—	—	—	x_7
010111	—	—	—	x_8
011000	—	—	—	x_9
011001	—	—	—	x_{10}
011010	—	—	—	x_{11}
011011	—	—	—	x_{12}
011100	—	—	—	x_{13}
011101	—	—	—	x_{14}
011110	—	—	—	x_{15}
011111	—	—	—	x_{16}
100000	$x_1/\sqrt{2}$	$x_2/\sqrt{2}$	—	—
100001	$x_2/\sqrt{2}$	$x_3/\sqrt{2}$	—	—
100010	$x_3/\sqrt{2}$	$x_4/\sqrt{2}$	—	—
100011	$x_4/\sqrt{2}$	$x_5/\sqrt{2}$	—	—
100100	$x_5/\sqrt{2}$	$x_6/\sqrt{2}$	—	—
100101	$x_6/\sqrt{2}$	$x_7/\sqrt{2}$	—	—
100110	$x_7/\sqrt{2}$	$x_8/\sqrt{2}$	—	—
100111	$x_8/\sqrt{2}$	$x_9/\sqrt{2}$	—	—
101000	$x_9/\sqrt{2}$	$x_{10}/\sqrt{2}$	—	—
101001	$x_{10}/\sqrt{2}$	$x_{11}/\sqrt{2}$	—	—
101010	$x_{11}/\sqrt{2}$	$x_{12}/\sqrt{2}$	—	—
101011	$x_{12}/\sqrt{2}$	$x_{13}/\sqrt{2}$	—	—
101100	$x_{13}/\sqrt{2}$	$x_{14}/\sqrt{2}$	—	—
101101	$x_{14}/\sqrt{2}$	$x_{15}/\sqrt{2}$	—	—
101110	$x_{15}/\sqrt{2}$	$x_{16}/\sqrt{2}$	—	—
101111	$x_{16}/\sqrt{2}$	$x_1/\sqrt{2}$	—	—
110000	—	—	$x_1/\sqrt{2}$	$x_2/\sqrt{2}$
110001	—	—	$x_2/\sqrt{2}$	$x_3/\sqrt{2}$
110010	—	—	$x_3/\sqrt{2}$	$x_4/\sqrt{2}$
110011	—	—	$x_4/\sqrt{2}$	$x_5/\sqrt{2}$

Table 6 continued

Possible groups of $\log_2 MN_i(6)$ bits/channel/use	$Tx1$	$Tx2$	$Tx3$	$Tx4$
110100	–	–	$x_5/\sqrt{2}$	$x_6/\sqrt{2}$
110101	–	–	$x_6/\sqrt{2}$	$x_7/\sqrt{2}$
110110	–	–	$x_7/\sqrt{2}$	$x_8/\sqrt{2}$
110111	–	–	$x_8/\sqrt{2}$	$x_9/\sqrt{2}$
111000	–	–	$x_9/\sqrt{2}$	$x_{10}/\sqrt{2}$
111001	–	–	$x_{10}/\sqrt{2}$	$x_{11}/\sqrt{2}$
111010	–	–	$x_{11}/\sqrt{2}$	$x_{12}/\sqrt{2}$
111011	–	–	$x_{12}/\sqrt{2}$	$x_{13}/\sqrt{2}$
111100	–	–	$x_{13}/\sqrt{2}$	$x_{14}/\sqrt{2}$
111101	–	–	$x_{14}/\sqrt{2}$	$x_{15}/\sqrt{2}$
111110	–	–	$x_{15}/\sqrt{2}$	$x_{16}/\sqrt{2}$
111111	–	–	$x_{16}/\sqrt{2}$	$x_1/\sqrt{2}$

16 QAM points used are

$X = [-3.0000 + 3.0000i, -3.0000 + 1.0000i, -3.0000 - 1.0000i, -3.0000 - 3.0000i, -1.0000 + 3.0000i, -1.0000 + 1.0000i, -1.0000 - 1.0000i, -1.0000 - 3.0000i, 1.0000 + 3.0000i, 1.0000 + 1.0000i, 1.0000 - 1.0000i, 1.0000 - 3.0000i, 3.0000 + 3.0000i, 3.0000 + 1.0000i, 3.0000 - 1.0000i, 3.0000 - 3.0000i.]$

References

- Mesleh, R. Y., Haas, H., Sinanovic, S., Ahn, C. W., & Yun, S. (2008). Spatial modulation. *IEEE Transactions on Vehicular Technology*, 57(4), 2228–2241.
- Di Renzo, M., Haas, H., Ghrayeb, A., Sugiura, S., & Hanzo, L. (2014). Spatial modulation generalized for MIMO: Opportunities challenges and implementation. *Proceedings of the IEEE*, 102(1), 56–103.
- Younis, A. (2013). Spatial modulation: Theory to practice. (Ph.D thesis, The University of Edinburgh).
- Luna-Rivera, J. M. & Gonzalez-Perez, M. G. (2012). An improved spatial modulation scheme for MIMO channels. *EuCAP*.
- Luna-Rivera, J. M., Campos-Delgado, D. U., Gonzalez-Perez, M. G. (2013). Constellation design for spatial modulation. In *The 2013 iberoamerican conference on electronics engineering and computer science*, Elsevier.
- Cheng, C. C., Sari, H., Sezginert, S., Su, Y. T. (2014). Enhanced spatial modulation with multiple constellations. In *IEEE international black sea conference on communications and networking (BlackSeaCom)*.
- Cheng, C. C., Sari, H., Sezginer, S., & Su, Y. T. (2015). Enhanced spatial modulation with multiple signal constellations. *IEEE Transactions on Communications*, 63(6), 2237–2248.
- Mesleh, R., Ikki, S. S., & Aggoune, H. M. (2014). Quadrature Spatial Modulation. *IEEE Transactions on Vehicular Technology*, 64, 1. doi:10.1109/TVT.2014.2344036.
- Mesleh, R., Di Renzo, M., Haas, H., & Grant, P. M. (2010). Trellis coded spatial modulation. *IEEE Transactions on Wireless Communication*, 9(7), 2349–2361.
- Jeganathan, J., Ghrayeb, A., & Szczecinski, L. (2008). Spatial modulation: Optimal detection and performance analysis. *IEEE Communications Letters*, 12(8), 545–547.
- Mesleh, R. et.al. (2009) On the performance of trellis coded spatial modulation. *ITG workshop on smart antennas*, Berlin Germany.
- Afana, A., Atawi, I., Ikki, S. & Mesleh, R. (2015) Energy efficient quadrature spatial modulation MIMO cognitive radio systems with imperfect channel estimation. In *IEEE international conference on ubiquitous wireless broadband (ICUWB)* (pp. 1–5).
- Mesleh, R., Ikki, S. S., & Aggoune, H. M. (2015). Quadrature spatial modulation. *IEEE Transactions on Vehicular Technology*, 64(6), 2738–2742.
- Proakis, J. G. (2000). *Digital communications* (4th ed.). New York: McGraw–Hill.
- Mobile Broadband Evolution Towards 5G: 3GPP Rel-12 & Rel-13 and Beyond 2015.

16. Hedayat, A., Shah, H., & Nosratinia, A. (2005). Analysis of space-time coding in uncorrelated fading channels. *IEEE Transactions on Wireless Communications*, 4(6), 2882–2891.
17. Forenza, A. Love, D., Heath, R. Jr. (2004). A low complexity algorithm to simulate the spatial covariance matrix for clustered MIMO channel models. In *IEEE vehicular technology conference—VTC 2004-Fall, Los Angeles, CA, USA, May, 2004* (pp. 889–893).
18. MacLeod, H., Loadman, C., Chen, Z. (2005). Experimental studies of the 2.4-GHz ISM wireless indoor channel. In *Proceedings of the 3rd annual communication networks and services research conference (CNSR'05)*.
19. Duman, T. M., & Ghayeb, A. (2007). *Coding for MIMO communication systems*. Hoboken: Wiley.
20. Zelst and, A. V. & Hammerschmidt, J. S. (2002) A single coefficient spatial correlation model for multiple-input multiple-output (MIMO) radio channels. In *27th general assembly of the international union of radio science (URSI), Maastricht, The Netherlands, Aug. 17–24 2002* (pp. 1–4).
21. Mesleh, R. Y. (2007) Spatial Modulation: A spatial multiplexing technique for efficient wireless data transmission. (Ph.D Thesis, School of Engineering and Science Jacobs University).



G. D. Goutham Simha received his M.Tech degree in digital electronics and communications from Dayananda Sagar College of engineering, Bengaluru in 2010. Currently he is a Research scholar in the Department of Electronics and Communication Engineering, National Institute of Technology Karnataka, India. His areas of interest are: MIMO Wireless communications, Optical Wireless communications and Error Control Coding.



Shriharsha Koila Received his B.E. degree in Electronics and Communication Engineering from Malnad College of Engineering, Hassan in 2012 and M.Tech degree from National Institute of Technology Karnataka in 2015. His research interests are in Wireless Communications with emphasis on Error Control Coding applications.



N. Neha received his M Tech Research degree in Communication Engineering from the National Institute of Technology Karnataka, India in 2015. Currently working as Engineer at Qualcomm India Pvt limited, Hyd. Her areas of interest are: Wireless Communication, IoE and Error control coding.



M. A. N. S. Raghavendra received his M Tech degree in Communication Engineering from the National Institute of Technology Karnataka, India in 2013. Currently he is a Research scholar in the Department of Electronics and Communication Engineering, National Institute of Technology Karnataka, India. His areas of interest are: Free Space Optic communications and Error control coding.



U. Sripathi received his Ph.D. degree from Indian Institute of Science, Bangalore in 2005. He is currently serving as a Professor in the department of Electronics and Communication Engineering, National Institute of Technology Karnataka, India. His areas of interest are: Theory and Applications of Error Control Codes, Wireless Communications and Free Space Optical Systems.